Observation of infinite-range intensity correlations near the 3D Anderson localization transition

W.K. Hildebrand,[1] A. Strybulevych,[1] S.E. Skipetrov,[2] B.A. van Tiggelen,[2] and J.H. Page[1,*]

[1] *Department of Physics and Astronomy, University of Manitoba, Winnipeg, Canada*
[2] *Université Grenoble 1/CNRS, LPMMC UMR 5493, B.P. 166, 38042 Grenoble, France*

(Dated: March 29, 2013)

We report measurements and theory for long-range intensity correlations near the Anderson transition of classical waves in a three-dimensional disordered material. Our ultrasonic experiments are designed to unambiguously detect a recently predicted infinite-range C_0 contribution, due to local density of states fluctuations near the source. We find that these C_0 correlations, in addition to C_2 and C_3 contributions, are significantly enhanced near mobility edges. Separate measurements of the inverse participation ratio reveal a link between C_0 and the anomalous dimension Δ_2, implying that C_0 may also be used to explore the critical regime of the Anderson transition.

PACS numbers: 42.35.Cg, 42.25.Dd, 43.20.Gp, 71.23.An, 64.60.al

Wave transport in strongly scattering disordered systems continues to reveal remarkable phenomena that challenge our understanding of wave physics. In addressing these challenges, much can be learned by investigating the statistics and correlations of the randomly fluctuating transmitted intensity, or speckle pattern. Intensity correlations of different kinds have been predicted and observed for classical waves under various conditions: either short or long range (C_1, C_2, or C_3), and in either frequency, position or angle [1–7]. Also, correlations in polarization [8] or phase [9] have been investigated theoretically and experimentally. For some time, there have been speculations about a new kind of "C_0" correlation in the speckle pattern, with infinite range, caused by scattering in the proximity of the source [10, 11]. It was later shown that this speckle correlation is closely related to fluctuations in the local density of states (LDOS) of the waves in a random medium [12]. This quantity is very actively studied both theoretically [13] and experimentally [14–17]. Around the mobility edge (ME) of a three-dimensional (3D) disordered sample, the normalized variance of LDOS fluctuations is predicted to be of order unity. They are also expected to become dependent on the sample size at, and below, the ME, due to the presence of states with localized or fractal spatial structure. Recent theoretical studies even report the variance of LDOS fluctuations to behave critically, i.e. as a one-parameter scaling function of sample size and localization length [18, 19], which means they constitute a new tool to provide insight into the Anderson transition. However, despite the profusion of results concerning LDOS fluctuations, no direct experimental evidence of C_0 intensity correlations has been reported so far [20].

In this Letter, we present the first direct experimental evidence of infinite-range (C_0) spatial and frequency correlations of the intensity near the Anderson transition of a disordered, strongly scattering 3D material. The experiments were performed using ultrasonic techniques on samples in which 3D Anderson localization of ultrasound has been demonstrated previously [21]. Comparison of experiment with theory, coupled with complementary measurements designed to suppress infinite-range correlations when desired, allows the C_0 contribution to the correlations to be clearly separated from the other contributions (C_1, C_2, or C_3), unambiguously revealing the presence of large infinite-range correlations. We observe that these correlations grow dramatically near the expected mobility edges in our samples. Motivated by the prediction that the LDOS fluctuations are closely related to multifractality of the wave functions through the $q = 2$ generalized inverse participation ratio (gIPR) [15, 19], we measure the anomalous dimension Δ_2 for our samples in independent experiments and find good correspondence between this quantity and measured C_0 correlations. This clearly demonstrates the link between multifractality, C_0, and the LDOS fluctuations.

The samples investigated are disordered elastic networks of aluminum beads, weakly brazed together to form slabs [21]. The monodisperse beads are 4 mm in diameter, and the samples have 45% porosity, consistent with random loose packing. This porous mesoscale structure leads to very strong scattering with low absorption in the frequency range investigated ($\sim$ 0.5–2.5 MHz), a crucial feature for the observation of 3D Anderson localization of ultrasound in this material. The mesoscale structure also leads to high contrast in the density of states of the aluminum matrix compared to that of the pores—yet another reason for anticipating strong fluctuations of the LDOS. The samples were waterproofed so that the experiments could be performed in a water tank with either vacuum or air in the pores, thereby ensuring that the detected transmitted waves had traveled only through the aluminum bead network.

In our experiments, a broadband ultrasonic pulse is incident on the sample, and the transmitted waves are measured in the near field. The pulse is generated by a piezoelectric transducer, and is tightly focused to a spot approximately a wavelength in size on the input

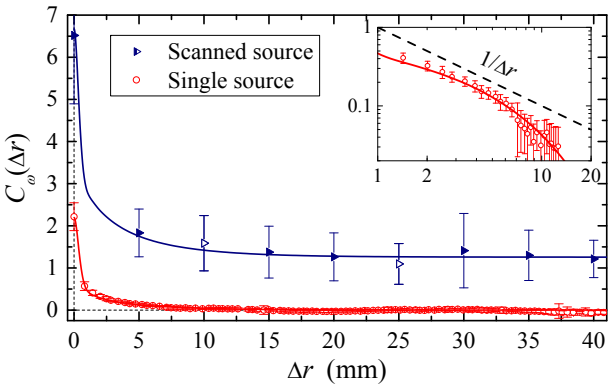

FIG. 1. (color online) Spatial intensity correlations for the two types of experiments at 2.4 MHz. The scanned-source data show convincing evidence of infinite-range (C_0) correlations, which are suppressed when only a single source point is used. Lines are theoretical fits using the values of parameters given in Table I. The inset shows the single-source data on a log-log scale in order to reveal the extent to which the expected $1/\Delta r$ dependence is observed for C_2 and C_3 at intermediate length scales. Data have been averaged over a bandwidth of 750 kHz, and the error bars are the standard deviations associated with the data's statistical fluctuations, which are observed to be inherently large near the Anderson transition. (The open symbols for the scanned-source data represent positions where the measurements are not as reliable because of a smaller signal-to-noise ratio.)

face of the sample. The transmitted pressure is detected by a sub-wavelength hydrophone, typically placed less than 1 mm from the sample surface (within one wavelength in water). To capture contributions to C_0 due to LDOS fluctuations at both the focal point of the incident wave (source point) and the detector, we scan both the source and detector over the surface of the sample. The recorded pressure fields $p(\mathbf{r},t)$ are Fourier transformed to obtain the intensity $I(\mathbf{r},\omega) \propto |p(\mathbf{r},\omega)|^2$ as a function of frequency for each pair of source and detector positions. The correlation function of intensity is calculated as

$$C_\omega(\Delta r,\Omega) = \frac{\langle \delta I(\mathbf{r},\omega-\frac{1}{2}\Omega)\delta I(\mathbf{r}+\Delta\mathbf{r},\omega+\frac{1}{2}\Omega)\rangle}{\langle I(\mathbf{r},\omega-\frac{1}{2}\Omega)\rangle\langle I(\mathbf{r}+\Delta\mathbf{r},\omega+\frac{1}{2}\Omega)\rangle}, \quad (1)$$

where the angular brackets denote ensemble averaging and $\delta I = I - \langle I\rangle$ is the fluctuation of intensity. Ensemble averaging is done by scanning over many source and detector positions corresponding to the same Δr. For comparison, experiments with a single (stationary) point source were also performed, in which case the ensemble averaging was done only over all possible detector positions; this suppresses C_0 correlations due to LDOS fluctuations at the source. In what follows we will study spatial correlations $C_\omega(\Delta r) = C_\omega(\Delta r, 0)$ and frequency correlations $C_\omega(\Omega) = C_\omega(0,\Omega)$ separately.

Figure 1 shows the spatial correlations measured near $f = \omega/2\pi = 2.4$ MHz, the frequency at which Anderson localization of elastic waves was demonstrated in this sample [21]. For both types of experiments, the correlations decay rapidly at small Δr due to C_1, with a slower decay due to C_2 and C_3 that extends out to $\Delta r \sim 10$ mm, beyond which $C_\omega(\Delta r)$ becomes independent of distance. For the data where the source position is varied, an asymptotic value of order unity is seen for the correlations, showing clear evidence of a C_0 term due to LDOS fluctuations at the source. By contrast, no infinite-range correlations are seen for the single-source data, consistent with the fact that the LDOS at the source position does not fluctuate in this case.

To gain further insight into this behavior, we compare our experimental data with theoretical calculations. We compute C_1, C_2, C_3, and C_0 correlation functions assuming weak disorder and write the full correlation $C_\omega(\Delta r)$ as a function of three fit parameters: A, $C_0^{(\mathrm{in})}$, and $C_0^{(\mathrm{out})}$. The parameter A quantifies the magnitude of C_2 and C_3 correlations, $C_0^{(\mathrm{in})}$ characterizes the magnitude of the genuine C_0 correlation due to the LDOS fluctuations at the source point, and $C_0^{(\mathrm{out})}$ measures the amplitude of the short-range contribution to C_0 due to scattering in the vicinity of both detectors when the latter are close to each other [22]. $C_0^{(\mathrm{in})}$ is the asymptotic value of $C_\omega(\Delta r)$ for $\Delta r \to \infty$. The solid lines in Fig. 1 show the results of performing a *joint* weighted fit of these theoretical predictions to both the single- and scanned-source data at each frequency, thereby determining the values of the parameters shown in Table I. In these fits, we account for the fact that $C_0^{(\mathrm{in})}$ contributes only to the scanned-source correlations and set $C_0^{(\mathrm{in})} = 0$ for fitting the single-source data; also, since the detector geometry is the same for both experiments, $C_0^{(\mathrm{out})}$ is constrained to have a common value for the two curves. Note that for white-noise uncorrelated disorder and point-like source and detector in an infinite disordered medium, $C_0^{(\mathrm{in})} = C_0^{(\mathrm{out})} = \pi/k\ell$, where k is the wavenumber in the medium and ℓ is the mean free path [10]. In our experiments, however, both the source and detector have finite extent (which may differ from each other), and the finite size of the aluminum beads inevitably results in some short-range structural correlations. Therefore, we expect in general that $C_0^{(\mathrm{in})} \neq C_0^{(\mathrm{out})} \neq \pi/k\ell$ [11]. Figure 1 provides strong evidence that the large asymptotic value of $C_\omega(\Delta r \to \infty) = C_0^{(\mathrm{in})} \sim 1$ for the scanned-source experiment is due to C_0 correlations.

Similar behavior, with $C_0^{(\mathrm{in})} \sim 1$, is observed over a broad frequency range from 1.6 to 2.8 MHz, where independent measurements of the dynamic transverse confinement of the transmitted intensity [21] indicate that ultrasound is still localized, with similar values of the localization length ξ ($\xi \approx L = 14.5$ mm for this sample in this frequency range). At lower frequencies, at least one ME must exist, since previous measurements on

TABLE I. Fit parameters, with uncertainties in parentheses. The uncertainties are given by the standard deviation of the parameters. For a point source and detector, the normalized variance, $C(0,0)$, depends on all three parameters as $C(0,0) = 1 + 2[A + C_0^{(\mathrm{in})} + C_0^{(\mathrm{out})}]$. By contrast, the infinite range contributions depend independently on the different contributions to C_0, with the asymptotic values of the scanned-source $C(\Delta r, 0)$, the single-source $C(0,\Omega)$ and the scanned-source $C(0,\Omega)$ being equal to $C_0^{(\mathrm{in})}$, $C_0^{(\mathrm{out})}$, and $C_0^{(\mathrm{in})} + C_0^{(\mathrm{out})}$, respectively.

Parameter	2.4 MHz	0.97 MHz	1.07 MHz	1.11 MHz
Spatial correlations				
A (single)	0.50 (0.02)	0.48 (0.02)	1.29 (0.04)	1.59 (0.06)
A (scanned)	2 (1)	0.8 (0.2)	6 (1)	6 (3)
$C_0^{(\mathrm{in})}$	1.3 (0.2)	0.42 (0.02)	1.06 (0.08)	7.8 (0.5)
$C_0^{(\mathrm{out})}$	0.4 (0.2)	0.8 (0.2)	1.5 (0.4)	7 (1)
Frequency correlations				
A (single)		0.2 (0.2)	0.8 (0.3)	
A (scanned)		0.7 (0.1)	5.2 (0.8)	
$C_0^{(\mathrm{in})}$		0.32 (0.03)	0.9 (0.3)	
$C_0^{(\mathrm{out})}$		0.62 (0.06)	1.3 (0.1)	
$\Omega_{\mathrm{Th}}/2\pi$ (kHz)		4.35 (0.09)	7.2 (0.1)	

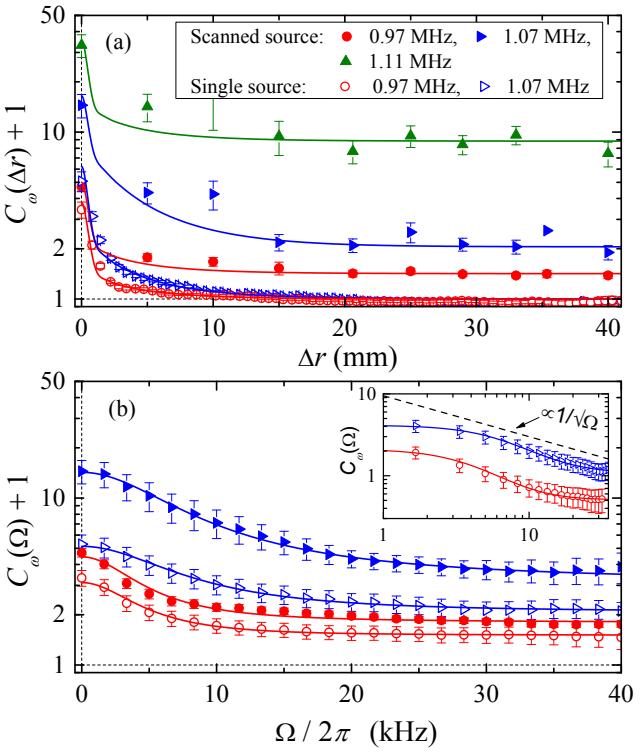

FIG. 2. (color online) Spatial (a) and frequency (b) correlations measured near 1 MHz, showing the increase of long-range correlations near a mobility edge. The inset shows the characteristic $1/\sqrt{\Omega}$ behavior expected for C_2 and C_3 correlations. For both plots, data have been averaged over a bandwidth of 25 kHz, except at the highest frequency (1.11 MHz), where the data are changing too rapidly with frequency to be meaningfully averaged. These rapid variations with frequency near 1.11 MHz also complicate measurements of frequency correlations, which are therefore not shown here. The error bars are calculated as in Fig. 1. Lines show the fits using the parameters given in Table I.

these samples revealed that ultrasound propagates diffusively at the much lower frequency of 200 kHz [21]. To investigate the long-range correlations as a ME is approached, experiments were performed at intermediate frequencies, between these well established diffusive and localized regimes [21], with representative data at frequencies near 1 MHz being presented in Fig. 2. Both spatial and frequency correlations increase significantly with frequency when a ME, which we estimate to be at approximately 1.1 MHz, is approached. In particular, the asymptotic value of the scanned-source spatial correlations, $C_0^{(\mathrm{in})}$, increases from 0.4 to almost 8 over the range of frequencies illustrated in Fig. 2(a).

The frequency correlations also show large increases in C_0 over this frequency range [see Fig. 2(b)] [23]. $C_\omega(\Omega)$ contains infinite-range contributions from scattering both near the source and near the detector, i.e. both $C_0^{(\mathrm{in})}$ and $C_0^{(\mathrm{out})}$ contribute to the asymptotic value of $C_\omega(\Omega)$ for large Ω [22]. The single-source measurements (which suppress $C_0^{(\mathrm{in})}$) show that $C_0^{(\mathrm{out})}$ increases from 0.6 to 1.3 between 0.97 and 1.07 MHz. By comparing the best-fit values (see Table I), we see that for the scanned-source case, $C_0^{(\mathrm{in})}$ and $C_0^{(\mathrm{out})}$ are of the same order of magnitude, as could be expected from the roughly symmetric arrangement of the experiment [24].

The C_2 and C_3 correlations, quantified by the parameter A, also increase with frequency around 1 MHz, as found from the data for both spatial and frequency correlations (see Fig. 2 and Table I). Because $A \propto 1/(k\ell^*)^2$ to leading order [22], where ℓ^* is the transport mean free path, the increase of A corresponds to a decrease of $k\ell^*$ as the ME is approached. In addition, the values of A found from the fits are always larger in the scanned-source case. Keeping the source fixed not only suppresses $C_0^{(\mathrm{in})}$ but also reduces the magnitude of long-range C_2 and C_3 correlations because the latter contain contributions from scattering in the vicinity of the source. This effect does not preclude the clear identification of C_0 that stands out by its infinite range in both space and frequency.

The frequency dependence of the asymptotic value of the spatial intensity correlation function between 0.6 and 1.4 MHz is shown in Fig. 3(a). These data are the average of the measured correlations for Δr between 25 and 50 mm, where $C_\omega(\Delta r)$ is found to be independent of distance, providing accurate measurements of $C_0(\Delta r \to \infty) = C_0^{(\mathrm{in})}$ when the source is scanned. It in-

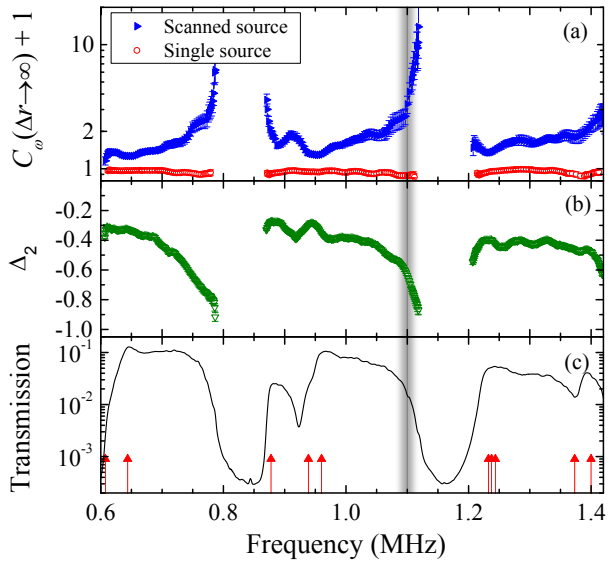

FIG. 3. (color online) (a) Frequency dependence of the asymptotic value of the spatial correlation $C_\omega(\Delta r \to \infty) = C_0^{(\mathrm{in})}$ for single and scanned point sources, (b) anomalous dimension Δ_2 of the gIPR for $q = 2$, and (c) the amplitude transmission coefficient. The arrows in (c) indicate the resonant frequencies of individual aluminum beads. $C_0^{(\mathrm{in})}$ and Δ_2 show large increases in magnitude near the upper band edges, where we expect mobility edges to occur. The grey vertical line indicates the location of the ME near 1.1 MHz, estimated from transverse confinement measurements .

creases rapidly with frequency near 0.78 and 1.11 MHz, reaching values up to 13 here, and even as high as 30 in other experiments—by far the largest values of C_0 ever reported. Comparison of these results with the amplitude transmission coefficient [Fig. 3(c)] reveals that the frequencies where C_0 increases rapidly coincide with the upper edges of pass bands in these disordered structures. In the band gaps, the transmission becomes too small to yield measurable long range correlations. As explained in Refs. [21, 25], these band gaps are not due to Bragg scattering, as in phononic crystals [26]. Instead, they arise between pass bands formed from coupled resonances of the beads when the coupling is sufficiently weak.

Near the upper edges of the pass bands, where the average density of states decreases, mobility edges between extended and localized states may be expected [27]. Evidence that mobility edges do indeed occur near these band edges has been obtained through separate measurements of increased spatial confinement of the transmitted intensity near the upper band edges relative to the pass band centers, using the method developed by Hu *et al.* [21]. This evidence is most compelling for the ME near 1.1 MHz, which is indicated by the vertical line in Fig. 3. Additional evidence can be inferred from the large increases that are found in the normalized intensity variance, $C_\omega(\Delta r = 0, \Omega = 0)$, near the upper band edges (e.g. Fig. 2 and Ref. [21]). Thus, the large increases in C_0 near 0.78 and 1.1 MHz must be due to large LDOS fluctuations near Anderson transitions in these samples, suggesting that C_0 is sensitive to critical effects.

This interpretation of the striking increase in C_0 near the band edges is further supported by measurements of the anomalous multifractal dimension Δ_2, which characterizes the length-scale dependence of the inverse participation ratio (IPR) $P_2 \sim L^{-d-\Delta_2}$ [28]. The significant decrease in Δ_2 with frequency near the upper band edges [Fig. 3(b)] is consistent with the predicted behavior near the Anderson transition, where Δ_2 should become increasingly negative, varying from 0 in the diffuse regime to -2 deep in localized regime [29]. Since the source and detector in our experiments are point-like, it is likely that a single mode dominates at any frequency, so we expect the IPR calculated from the intensity $I(\mathbf{r})$ and from the LDOS $\rho(\mathbf{r})$ to be equal [15, 19]. Then, $P_2 = L^{-d}\langle\rho^2\rangle/\langle\rho\rangle^2 = L^{-d}[C_0(\infty)+1]$, and we predict that $\log[C_0(\infty)+1] \propto -\Delta_2$. Within experimental error, the frequency dependencies of $C_\omega(\Delta r \to \infty) = C_0^{(\mathrm{in})}$ and Δ_2 [Figs. 3(a) and (b)] are consistent with this prediction. Thus, not only do the infinite-range correlations and the IPR show evidence of transitions from extended to localized behavior near the upper band edges, but the correspondence between these measurements verifies the link between C_0, LDOS fluctuations, and multifractality experimentally.

In conclusion, infinite-range intensity correlations have been measured directly in a strongly scattering 3D "mesoglass" for which Anderson localization of ultrasound was unambiguously demonstrated previously [21]. Measurements are consistent with the diagrammatic theory when large magnitudes of both long-range (C_2 and C_3) and infinite-range (C_0) terms are assumed. By varying the ultrasonic frequency, we have been able to investigate the growth not only of C_2 and C_3 but also of C_0 correlations as the Anderson transition is approached. Infinite-range correlations of order unity are found over a broad range of frequencies, reflecting the high LDOS contrast that can be achieved in our samples. The magnitude of these C_0 correlations is seen to increase dramatically near a ME. These C_0 results are mirrored by the frequency dependence of the anomalous dimension Δ_2, which characterizes the spatial structure of the inverse participation ratio. Our independent measurements of these two quantities establish a link between C_0 and Δ_2, revealing that C_0 can be used to probe the Anderson transition. The possibility of exploiting our findings to experimentally investigate critical behavior at the Anderson transition, by focusing on the possible one-parameter scaling of C_0 near the ME, is a promising new avenue for future research.

This work was supported by NSERC and by a PICS program of CNRS.

* john.page@ad.umanitoba.ca

[1] S. Feng, C. Kane, P. A. Lee and A. D. Stone, Phys. Rev. Lett. **61**, 834 (1988).

[2] E. Akkermans and G. Montambaux, *Mesoscopic Physics of Electrons and Photons* (Cambridge University Press, Cambridge, 2007).

[3] R. Berkovits and S. Feng, Phys. Rep. **238**, 135 (1994).

[4] J. F. de Boer, M. P. van Albada, and A. Lagendijk, Phys. Rev. B **45**, 658 (1992).

[5] M. C. W. van Rossum and T. M. Nieuwenhuizen, Rev. Mod. Phys. **71**, 313 (1999).

[6] F. Scheffold, W. Härtl, G. Maret, and E. Matijević, Phys. Rev. B **56**, 10942 (1997).

[7] P. Sebbah, R. Pnini, and A. Z. Genack, Phys. Rev. E **62**, 7348 (2000).

[8] A. A. Chabanov, N. P. Trégourès, B. A. van Tiggelen, and A. Z. Genack, Phys. Rev. Lett. **92**, 173901 (2004).

[9] M. L. Cowan, D. Anache-Ménier, W. K. Hildebrand, J. H. Page, and B. A. van Tiggelen, Phys. Rev. Lett. **99**, 094301 (2007).

[10] B. Shapiro, Phys. Rev. Lett. **83**, 4733 (1999).

[11] S.E. Skipetrov and R. Maynard, Phys. Rev. B **62**, 886 (2000).

[12] B.A. van Tiggelen and S.E. Skipetrov, Phys. Rev. E **73**, 045601 (2006).

[13] A. D. Mirlin, Phys. Rep. **326**, 259 (2000).

[14] M. D. Birowosuto, S. E. Skipetrov, W. L. Vos, and A. P. Mosk, Phys. Rev. Lett. **105**, 013904 (2010).

[15] V. Krachmalnicoff, E. Castanié, Y. De Wilde, and R. Carminati, Phys. Rev. Lett. **105**, 183901 (2010).

[16] R. G. S. El-Dardiry, S. Faez, and A. Lagendijk, Phys. Rev. A **83**, 031801 (2011).

[17] P. D. García, S. Stobbe, I. Söllner, and P. Lodahl, Phys. Rev. Lett. **109**, 253902 (2012).

[18] V. Dobrosavljević, A. A. Pastor, and B. K. Nikolić, Europhys. Lett. **62**, 76 (2003).

[19] N. C. Murphy, R. Wortis, and W. A. Atkinson, Phys. Rev. B **83**, 184206 (2011).

[20] The possible existence of small infinite-range contributions to C_2 and C_3 intensity correlation was pointed out in Ref. [8] for waves in quasi-1D disordered waveguides, but their origin was not identified with certainty.

[21] H. Hu, A. Strybulevych, J. H. Page, S. E. Skipetrov, and B. A.van Tiggelen, Nature Phys. **4**, 945 (2008).

[22] See the supplemental material at the end of this document.

[23] The fits of the frequency correlations are performed similarly to those of the spatial correlations, with the additional parameter Ω_{Th} also constrained to have the same value for both single- and scanned-source experiments.

[24] Note that when both spatial and frequency correlations are measured, the values of both $C_0^{(\mathrm{in})}$ and $C_0^{(\mathrm{out})}$ can be determined most robustly from the asymptotic values of the correlations. For example, the fitted values of $C_0^{(\mathrm{out})}$ measured from the frequency correlations, which contain an infinite-range contribution due to $C_0^{(\mathrm{out})}$, are more reliable than those measured from the spatial correlations.

[25] J. A. Turner, M. E. Chambers, and R. L. Weaver, Acustica **84**, 628 (1998).

[26] S. Yang, J. H. Page, Z. Liu, M. L. Cowan, C. T. Chan, and P. Sheng, Phys. Rev. Lett. **88**, 104301 (2002).

[27] S. John, Phys. Rev. Lett. **58**, 2486 (1987).

[28] S. Faez, A. Strybulevych, J. H. Page, A. Lagendijk, and B. A. van Tiggelen, Phys. Rev. Lett. **103**, 155703 (2009).

[29] F. Evers and A. D. Mirlin, Rev. Mod. Phys. **80**, 1355 (2008).

Supplemental material

INTRODUCTION

This document provides the summary of theoretical results that we used to fit the data in the main text of the paper. We compute the short-, long- and infinite-range correlation functions of intensity under assumption of weak disorder $k\ell \gg 1$, where k is the wave number and ℓ is the mean free path due to disorder.

SPATIAL CORRELATIONS

Definitions

We consider the spatial correlation function of intensity fluctuations $\delta I(\mathbf{r},\omega) = I(\mathbf{r},\omega) - \langle I(\mathbf{r},\omega)\rangle$:

$$C_\omega(\mathbf{r},\mathbf{r}') = \frac{\langle \delta I(\mathbf{r},\omega)\delta I(\mathbf{r}',\omega)\rangle}{\langle I(\mathbf{r},\omega)\rangle\langle I(\mathbf{r}',\omega)\rangle}. \tag{S1}$$

To lighten the notation, we will omit the subscript 'ω' from here on, keeping in mind that all measurements are performed for waves at the same frequency ω. Typically, $C(\mathbf{r},\mathbf{r}')$ is a decaying function of $\Delta r = |\mathbf{r}-\mathbf{r}'|$ with $C(\mathbf{r},\mathbf{r}'=\mathbf{r}) = \langle \delta I(\mathbf{r})^2\rangle/\langle I(\mathbf{r})\rangle^2$ being the normalized variance of intensity, and $C(\mathbf{r},\mathbf{r}') = 0$ in the absence of intensity correlations. It is convenient to split $C(\mathbf{r},\mathbf{r}')$ in several parts: $C = C_1 + C_2 + C_3 + C_0$, each of C_i originating from different physical processes [S1, S2].

Short-range correlation C_1

In the bulk of a disordered medium and far from boundaries, the short-range contribution to C is [S1, S3]

$$C_1^{\text{bulk}}(\mathbf{r},\mathbf{r}') = \left(\frac{\sin k\Delta r}{k\Delta r}\right)^2 \exp(-\Delta r/\ell), \tag{S2}$$

where $k = 2\pi/\lambda$, ℓ is the scattering mean free path. At the surface of a disordered sample, the spatial correlation C_1 is modified due to the anisotropic angular distribution of intensity [S4]:

$$C_1^{\text{surface}}(\mathbf{r},\mathbf{r}') = \left\{\frac{1}{\Delta+\frac{1}{2}}\left[\Delta\frac{\sin k\Delta r}{k\Delta r} + \frac{J_1(k\Delta r)}{k\Delta r}\right]\right\}^2 \times \exp(-\Delta r/\ell) = h(k\Delta r, k\ell), \tag{S3}$$

where $\Delta = z_0/\ell^*$ with z_0 the extrapolation length entering the boundary conditions for the average intensity, and we defined the function $h(k\Delta r, k\ell)$ that will be used in the following. This result is largely independent of the spatial extent of the source (plane wave, beam of finite size or point source) and has been tested experimentally [S5].

Long-range correlation C_2

In contrast to C_1, the long-range contribution C_2 depends on the spatial extent of the source. It is not easy to calculate for an arbitrary source. In addition, we have to make an assumption of weak disorder ($k\ell \gg 1$) to compute the diagrams corresponding to C_2.

Transmission of a plane wave through a slab. We assume that a slab of thickness $L \gg \ell$ and transverse extent $W \gg L$ is illuminated by a plane wave. The spatial correlation of intensity is calculated at the opposite side of the slab, as a function of transverse distance $\Delta r = |\mathbf{r}-\mathbf{r}'| \gg \ell^*$ [S6, S7]:

$$C_2^{\text{plane wave}}(\Delta r) = \frac{3}{2(k\ell^*)^2}\frac{\ell^*}{L}\left[\frac{L}{\Delta r} + F\left(\frac{\Delta r}{L}\right)\right] \simeq \begin{cases} \frac{3}{2(k\ell^*)^2}\frac{\ell^*}{\Delta r}, & \Delta r \ll L, \\ \propto e^{-\pi\Delta r/L}, & \Delta r > L, \end{cases} \tag{S4}$$

where

$$F(x) = \frac{1}{2}\int_0^\infty dq J_0(qx)\left(\frac{\sinh 2q - 2q}{\sinh^2 q} - 2\right), \tag{S5}$$

and ℓ^* is the transport mean free path.

Equation (S4) applies for $\Delta r \gg \ell^*$ only. It is clear that its divergence at $\Delta r \to 0$ is an artifact of approximations made during its derivation. Physically, we expect $C_2(\Delta r = 0) \simeq C_2(\Delta r = \ell^*)$. A more precise shape of $C_2(\Delta r)$ at small $\Delta r \lesssim \ell^*$ can be obtained by paying more attention to small q and avoiding the limit $q\ell^* \ll 1$ which is tacitly taken in the derivation of Eq. (S4). We then obtain a longer but more accurate expression for C_2:

$$C_2^{\text{plane wave}}(\Delta r) = \frac{3}{2(k\ell^*)^2}F_2\left(\frac{\Delta r}{L}, \frac{\ell^*}{L}\right), \tag{S6}$$

where

$$F_2(x,y) = \frac{y}{2}\int_0^\infty du \frac{J_0(ux)}{(uy\sinh u)^2}\left\{\sinh^2(uy) \times [\sinh[2u(1-y)] - 2u(1-y)] + \sinh^2[u(1-y)]\,[\sinh(2uy) - 2uy]\right\} \simeq \begin{cases} 1-y, & x = 0, \\ y/x, & y \ll x \ll 1, \\ \propto e^{-\pi x}, & x > 1. \end{cases} \tag{S7}$$

A comparison of Eqs. (S4) and (S6) is shown in Fig. S1. The latter equation, in contrast to Eq. (S4), allows us to obtain the value of C_2 for $\Delta r = 0$:

$$C_2^{\text{plane wave}}(\Delta r = 0) = \frac{3}{2(k\ell^*)^2}\left(1 - \frac{\ell^*}{L}\right). \tag{S8}$$

Point source in the infinite medium. Even if this geometry seems simple, the calculation of C_2 appears quite involved. If we define the center of mass

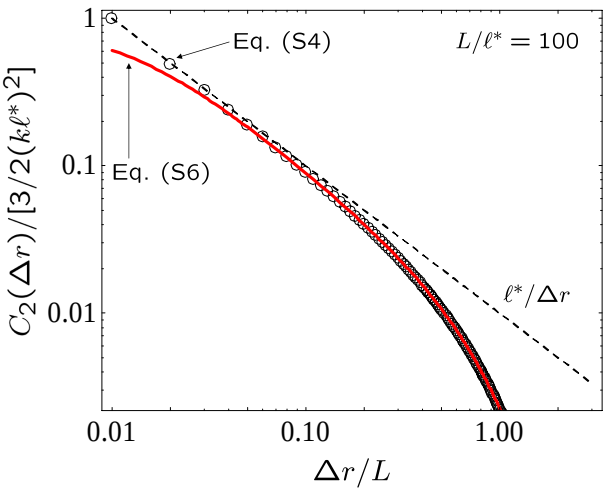

FIG. S1. Comparison of Eqs. (S4) (shown by circles) and (S6) (shown by the solid red line) for the long-range correlation function of intensity fluctuations. The dashed line shows $\ell^*/\Delta r$.

$\mathbf{R} = \frac{1}{2}(\mathbf{r}_1 + \mathbf{r}_2)$ and the difference $\Delta\mathbf{r} = \mathbf{r}_1 - \mathbf{r}_2$ coordinates, we can obtain simple results for $\Delta\mathbf{r} \perp \mathbf{R}$:

$$C_2^{\text{point source}}(\Delta r) \simeq \pm\frac{3}{2(k\ell^*)^2}\frac{\ell^*}{\Delta r}, \tag{S9}$$

with the '+' sign for $\Delta r \ll R$ and the '−' sign for $\Delta r \gg R$.

Transmission of a tightly focused beam through a slab. This situation is realized in our experiments and is somewhat intermediate with respect to the two previous cases (the sample is a slab, but the source is point-like). Because the results for the plane wave incident on a slab (S6) and the point source in the infinite medium (S9) coincide for $\ell^* < \Delta r < L$, we expect that the same result will also hold for the tightly focused beam. We will therefore use:

$$C_2^{\text{focused beam}}(\Delta r) \simeq \frac{3}{2(k\ell^*)^2} F_2\left(\frac{\Delta r}{L}, \frac{\ell^*}{L}\right), \quad \Delta r < L. \tag{S10}$$

For $\Delta r > L$, we expect $C_2^{\text{focused beam}}(\Delta r)$ to be different from both Eqs. (S6) and (S9), but because its magnitude is already small at such large distances, it will not play a significant role in the fits to the experimental data.

Short-range part of C_2. The calculation leading to Eqs. (S6), (S9) and (S10) also yields short-range terms that are rarely mentioned but exist. The full expression for C_2 including both long- and short-range contributions is

$$C_2^{\text{full}}(\Delta r) \simeq \frac{3}{2(k\ell^*)^2}\left[F_2\left(0, \frac{\ell^*}{L}\right) h(k\Delta r, k\ell) + F_2\left(\frac{\Delta r}{L}, \frac{\ell^*}{L}\right)\right]. \tag{S11}$$

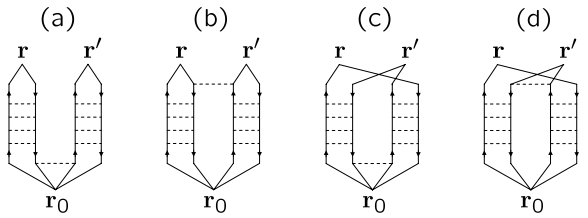

FIG. S2. Diagrams contributing to C_0 correlation function. $\mathbf{r}_0$ is the source position. The diagram (a) is the original long-range one [S2]; it is independent of $\Delta r = |\mathbf{r} - \mathbf{r}'|$. The diagram (b) is short-range. It was calculated in Ref. [S8]. The diagrams (c) and (d) are both short-range and were not considered previously. A complex conjugate diagram should be added to each of the diagrams.

Long-range correlation C_3

The calculation of the spatial C_3 correlation function for a beam focused on the surface of a 3D disordered slab is a complicated task that we did not succeed in accomplishing. However, the structure of the result may be anticipated from the diagrams involved in the calculation [S1]: we expect short- and long-range terms similar to C_2. The magnitude of C_3 is expected to be of order $1/(k\ell^*)^4$. Hence, an approximate expression for C_3 may be written as

$$C_3(\Delta r) \simeq \frac{\text{const}}{(k\ell^*)^4}\left[F_2\left(0, \frac{\ell^*}{L}\right) h(k\Delta r, k\ell) + F_2\left(\frac{\Delta r}{L}, \frac{\ell^*}{L}\right)\right]. \tag{S12}$$

Infinite-range correlation C_0

Similarly to C_2 and C_3, C_0 correlation also contains the 'interesting', infinite-range part and the 'trivial', short-range one. The full expression is found by summing the diagrams of Fig. S2:

$$C_0^{(a)}(\Delta r) = C_0^{(\text{in})}, \tag{S13}$$

$$C_0^{(b)}(\Delta r) = C_0^{(\text{out})}\frac{f_b(k\Delta r, k\ell)}{f_b(0, k\ell)}, \tag{S14}$$

$$C_0^{(c)}(\Delta r) = C_0^{(\text{in})} h(k\Delta r, k\ell), \tag{S15}$$

$$C_0^{(d)}(\Delta r) = C_0^{(\text{out})}\frac{f_d(k\Delta r, k\ell)}{f_d(0, k\ell)}, \tag{S16}$$

where $C_0^{(\text{in})}$ is the genuine, infinite-range correlation that survives at large Δr [S2]. It results from the scattering near the source and is related to the variance of the local density of states at $\mathbf{r}_0$ [S9]. In contrast, the terms (S14) and (S16), which are proportional to $C_0^{(\text{out})}$, result from the scattering near the detection points $\mathbf{r}_1$ and $\mathbf{r}_2$.

They are appreciable only at small $\Delta r = |\mathbf{r}_1 - \mathbf{r}_2|$. For the white-noise uncorrelated disorder, $C_0^{(\mathrm{in})} = C_0^{(\mathrm{out})} = \pi/k\ell$. In our experiment, the disorder is correlated and the symmetry between the 'point-like' excitation and the 'point-like' detection may be broken because neither is actually point-like and the effective sizes of the excitation and detection areas may differ, so that $C_0^{(\mathrm{in})} \neq C_0^{(\mathrm{out})} \neq \pi/k\ell$. Moreover, these parameters are not universal and will depend on the microscopic structure of the disordered sample [S10]. We use $C_0^{(\mathrm{in})}$ and $C_0^{(\mathrm{out})}$ as free fit parameters when comparing theory to the experimental data.

The functions $f_b(k\Delta r, k\ell)$ and $f_d(k\Delta r, k\ell)$ are rapidly decaying functions of $k\Delta r$:

$$\begin{aligned} f_b(k\Delta r, k\ell) = \frac{1}{2\pi k\Delta r}\mathrm{Re}\Big\{ i\int_0^\infty dx \frac{\sin x}{x} e^{-(i+1/k\ell)x} \\ \times \Big(\mathrm{Ei}[-(k\Delta r + x)/k\ell] \\ - \mathrm{Ei}[(2i - 1/k\ell)(k\Delta r + x)] \\ + \mathrm{Ei}[(2i - 1/k\ell)|k\Delta r - x|] \\ - \mathrm{Ei}[-|k\Delta r - x|/k\ell]\Big)\Big\}, \end{aligned} \tag{S17}$$

$$\begin{aligned} f_d(k\Delta r, k\ell) = \frac{1}{\pi k\Delta r}\int_0^\infty dx \frac{\sin^2 x}{x} e^{-x/k\ell} \\ \times \left[\mathrm{Ei}\left(-\frac{k\Delta r + x}{k\ell}\right) \right. \\ \left. - \mathrm{Ei}\left(-\frac{|k\Delta r - x|}{k\ell}\right)\right]. \end{aligned} \tag{S18}$$

The behavior of these functions is illustrated in Fig. S3.

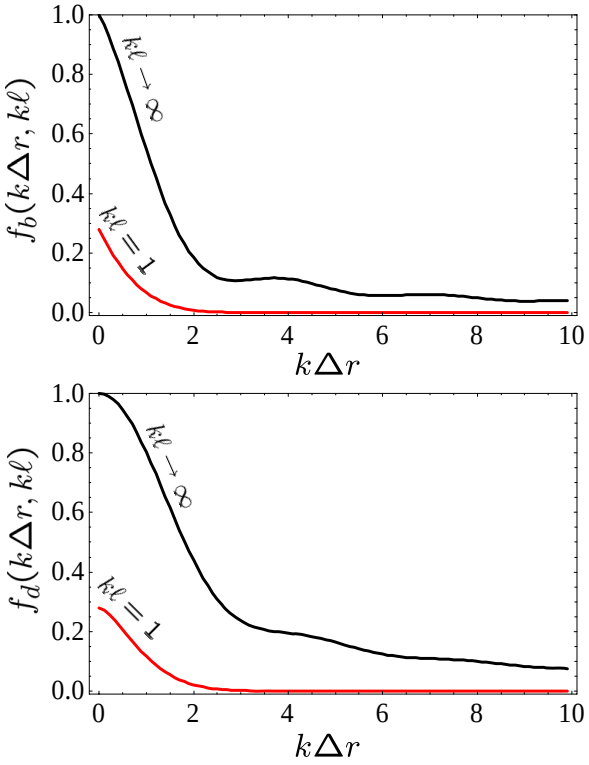

FIG. S3. Functions f_b and f_d describing the short-range part of C_0 correlation function.

Full expression for the correlation function

Adding up Eqs. (S3), (S11), (S12) and (S13)–(S16) we end up with an expression that can be used to fit experimental data:

$$\begin{aligned} C(\Delta r) = \left[1 + A + C_0^{(\mathrm{in})}\right] h(k\Delta r, k\ell) \\ + A \times \frac{F_2\left(\Delta r/L, \ell^*/L\right)}{F_2\left(0, \ell^*/L\right)} + C_0^{(\mathrm{in})} \\ + C_0^{(\mathrm{out})}\left[\frac{f_b(k\Delta r, k\ell)}{f_b(0, k\ell)} + \frac{f_d(k\Delta r, k\ell)}{f_d(0, k\ell)}\right], \end{aligned} \tag{S19}$$

where $A = [3/2(k\ell^*)^2 + \mathrm{const}/(k\ell^*)^4] F_2\left(0, \ell^*/L\right)$. A, $C_0^{(\mathrm{in})}$ and $C_0^{(\mathrm{out})}$ are the unknown fit parameters.

Accounting for the size of the detector

In the experiment, the acoustic field is measured very close to the sample surface with a disk-shaped hydrophone of radius $b = 0.2$ mm. In order to take into account the size of the hydrophone, we assume that the measured quantity is not the intensity $I(\mathbf{r})$ at a point $\mathbf{r}$ but the intensity averaged over a disk of radius b centered at $\mathbf{r}$:

$$\mathcal{I}(\mathbf{r}) = \frac{1}{\pi b^2}\int_{b(\mathbf{r})} I(\mathbf{r}')d^2\mathbf{r}', \tag{S20}$$

where $b(\mathbf{r})$ denotes a disk of radius b centered at $\mathbf{r}$. The correlation function of $\mathcal{I}(\mathbf{r})$ can be then obtained from the correlation of $I(\mathbf{r})$ by a double spatial integration:

$$\begin{aligned} C_{\mathcal{I}}(\Delta\mathbf{r} = \mathbf{r}_1 - \mathbf{r}_2) = \frac{1}{(\pi b^2)^2}\int_{b(\mathbf{r}_1)} d^2\mathbf{r}_1' \int_{b(\mathbf{r}_2)} d^2\mathbf{r}_2' \\ \times C_I(\Delta\mathbf{r}' = \mathbf{r}_1' - \mathbf{r}_2'). \end{aligned} \tag{S21}$$

FREQUENCY CORRELATIONS

Definitions

The frequency correlation function of intensity fluctuations $\delta I(\mathbf{r}, \omega) = I(\mathbf{r}, \omega) - \langle I(\mathbf{r}, \omega)\rangle$ is defined as

$$C_\omega(\mathbf{r}, \Omega) = \frac{\langle \delta I(\mathbf{r}, \omega + \frac{1}{2}\Omega)\, \delta I(\mathbf{r}, \omega - \frac{1}{2}\Omega)\rangle}{\langle I(\mathbf{r}, \omega)\rangle^2}, \tag{S22}$$

where we assume that the average intensity is independent of frequency in the frequency band under consideration: $\langle I(\mathbf{r},\omega+\frac{1}{2}\Omega)\rangle = \langle I(\mathbf{r},\omega-\frac{1}{2}\Omega)\rangle = \langle I(\mathbf{r},\omega)\rangle$. Once again, we will omit the subscript 'ω' of C from here on. The behavior of $C(\mathbf{r},\Omega)$ with Ω is similar to the behavior of the spatial correlation function $C(\Delta r)$ with Δr: it decays and has both short- and long-range parts.

Short-range correlation C_1

The short-range part of C can be easily calculated in transmission of a plane wave through a slab of thickness L [S1, S5]:

$$C_1(\Omega) = \left| \frac{L}{\ell^*} \times \frac{\sinh^2(\alpha\ell^*)}{\alpha\ell^* \sinh \alpha L} \right|^2, \tag{S23}$$

where $\alpha L = \pi\sqrt{i\Omega/\Omega_{\rm Th}}$, $\Omega_{\rm Th} = \pi^2 D/L^2$ is the Thouless frequency, D is the diffusion coefficient of the wave, and we neglected corrections due to boundary conditions, assuming $L \gg \ell^*$, z_0.

For a point source at the origin in the infinite medium we have

$$C_1(\mathbf{R},\Omega) = \left|\exp\left(-\alpha R\right)\right|^2, \tag{S24}$$

with similar definitions $\alpha R = \pi\sqrt{i\Omega/\Omega_{\rm Th}}$, $\Omega_{\rm Th} = \pi^2 D/R^2$.

Both correlation functions (S23) and (S24) oscillate and decay roughly exponentially with $\sqrt{\Omega/\Omega_{\rm Th}}$, so that no correlation is left for $\Omega \gg \Omega_{\rm Th}$. We will adopt Eq. (S23) in the following.

Long-range correlation C_2

Transmission of a plane wave through a slab. From a calculation following Refs. [S7, S11] we found the following result:

$$C_2^{\text{plane wave}}(\Omega) = \frac{3}{2(k\ell^*)^2} F_2\left(\alpha L, \frac{\ell^*}{L}\right), \tag{S25}$$

where

$$F_2\left(\alpha L, \frac{\ell^*}{L}\right) = \frac{1}{2}\frac{L}{\ell^*}\int_0^\infty du\; u\; f\left(\frac{u}{L}, \alpha L, \frac{\ell^*}{L}\right), \tag{S26}$$

$$\begin{aligned} f\left(q, \alpha L, \frac{\ell^*}{L}\right) = \frac{4}{L}\Bigg[& \int_0^{\ell^*} dz \left(\frac{\sinh qz\ \sinh q\ell^*}{q\sinh qL} \right. \\ & \left. \times \left| \frac{\partial}{\partial z} \frac{\sinh \alpha z\ \sinh \alpha(L-\ell^*)}{\alpha\ell^*\ \sinh \alpha L} \right| \right)^2 \\ & + \int_{\ell^*}^{L-\ell^*} dz \left(\frac{\sinh qz\ \sinh q\ell^*}{q\sinh qL} \right. \\ & \left. \times \left| \frac{\partial}{\partial z} \frac{\sinh \alpha\ell^*\ \sinh \alpha(L-\ell^*)}{\alpha\ell^*\ \sinh \alpha L} \right| \right)^2 \\ & + \int_{L-\ell^*}^{L} dz \left(\frac{\sinh q(L-\ell^*)\ \sinh q(L-z)}{q\sinh qL} \right. \\ & \left. \times \left| \frac{\partial}{\partial z} \frac{\sinh \alpha\ell^*\ \sinh \alpha(L-\ell^*)}{\alpha\ell^*\ \sinh \alpha L} \right| \right)^2 \Bigg]. \end{aligned} \tag{S27}$$

Integrations in this equation can be carried out analytically, resulting in a long expression that we do not reproduce here. Then the integral in Eq. (S26) can be calculated numerically.

In the limit of a thick slab $L \gg \ell^*$, Eq. (S25) yields a function that depends mainly on $\Omega/\Omega_{\rm Th}$ as far as $\Omega/\Omega_{\rm Th} \lesssim 1$, see Fig. S4 (top). In the limit of large $\Omega/\Omega_{\rm Th} \to \infty$ we find

$$C_2^{\text{plane wave}}(\Omega) \propto C_2^{\text{plane wave}}(0) \times \frac{\ell^*}{L}\sqrt{\frac{\Omega_{\rm Th}}{\Omega}}, \tag{S28}$$

as illustrated in Fig. S4 (bottom).

Point source in the infinite medium. Here we need to introduce a spatial cut-off $\sim \ell^*$ to avoid the path crossing (Hikami box) being closer than ℓ^* to the detector. The results then should be understood as depending on the precise value of this cutoff:

$$C_2^{\text{point source}}(\Omega) \simeq \frac{3}{4(k\ell^*)^2} F_2\left(\alpha R, \frac{\ell^*}{R}\right), \tag{S29}$$

where

$$\begin{aligned} F_2\left(\alpha R, \frac{\ell^*}{R}\right) = 2\frac{\ell^*}{R}\Bigg\{ & \int_0^{1-\ell^*/R} dx \frac{\exp[-2\mathrm{Re}(\alpha R)x]}{(1-x^2)^2} \\ & + \int_{1+\ell^*/R}^{\infty} dx \frac{\exp[-2\mathrm{Re}(\alpha R)x]}{(1-x^2)^2} \Bigg\}. \end{aligned} \tag{S30}$$

In the limit of $R \gg \ell^*$ that is of interest for us here, we

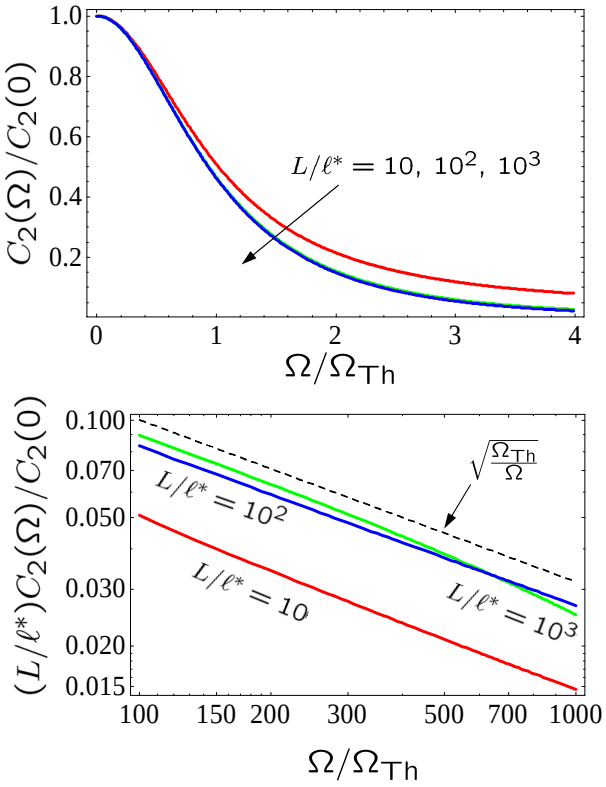

FIG. S4. Frequency correlation of intensity fluctuations C_2 in transmission of a plane wave through a disordered slab for small (top) and large (bottom) values of Ω.

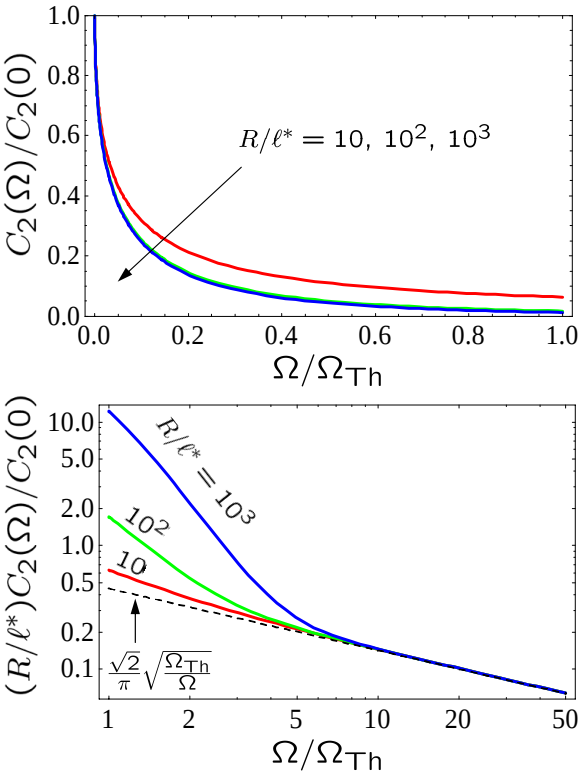

FIG. S5. Frequency correlation of intensity fluctuations C_2 at a distance R from a point source in the infinite medium for small (top) and large (bottom) values of Ω.

have

$$F_2\left(0, \frac{\ell^*}{R}\right) = 1, \tag{S31}$$

$$F_2\left(\alpha R, \frac{\ell^*}{R}\right) = \frac{\ell^*}{R} \times \frac{1}{\mathrm{Re}(\alpha R)}, \quad \Omega \gg \Omega_{\rm Th} \tag{S32}$$

The behavior of C_2 at small and large Ω is illustrated in Fig. S5.

Transmission of a tightly focused beam through a slab. We assume that the C_2 correlation function for a beam focused on the surface of a disordered slab is similar to the one for the plane wave, except for the magnitude of C_2 [S11]:

$$C_2^{\text{focused beam}}(\Omega) \simeq \frac{\text{const}}{(k\ell^*)^2} F_2\left(\alpha L, \frac{\ell^*}{L}\right), \tag{S33}$$

with $F_2(\alpha L, \ell^*/L)$ defined by Eq. (S26).

Infinite-range correlation C_0

The frequency dependence of the C_0 correlation function is obtained by calculating the diagrams of Fig. S6.

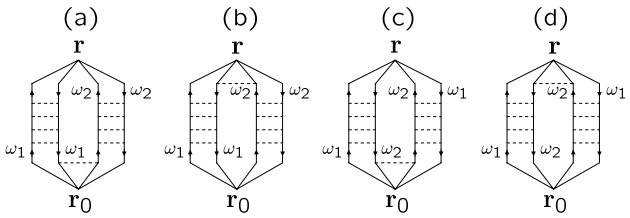

FIG. S6. Diagrams contributing to C_0 correlation function. $\mathbf{r}_0$ is the source position; $\omega_{1,2} = \omega \pm \frac{1}{2}\Omega$. The diagrams (a) and (b) are independent of $\Omega = \omega_1 - \omega_2$ as far as $|\Omega| \ll \omega_{1,2}$. A complex conjugate diagram should be added to each of the diagrams.

We obtain:

$$C_0^{(a)}(\Omega) = C_0^{(\text{in})}, \tag{S34}$$

$$C_0^{(b)}(\Omega) = C_0^{(\text{out})}, \tag{S35}$$

$$C_0^{(c)}(\Omega) = C_0^{(\text{in})} C_1(\Omega), \tag{S36}$$

$$C_0^{(d)}(\Omega) = C_0^{(\text{out})} C_1(\Omega). \tag{S37}$$

Full expression for the correlation function

Adding up all the contributions and assuming (as in the case of spatial correlations) that the behavior of C_3 as a function of frequency is similar to that of C_2, we finally find the full expression for the frequency correlation function:

$$C(\Omega) = \left[1 + C_0^{(\mathrm{in})} + C_0^{(\mathrm{out})}\right] C_1(\Omega) + 2A \times \frac{F_2(\alpha L, \ell^*/L)}{F_2(0, \ell^*/L)} + C_0^{(\mathrm{in})} + C_0^{(\mathrm{out})}, \quad \text{(S38)}$$

where $A \sim 1/(k\ell^*)^2$. Note that the constants A and $C_0^{(\mathrm{in,out})}$ here should be the same as in Eq. (S19) for the spatial correlation.

* john.page@ad.umanitoba.ca

[S1] E. Akkermans and G. Montambaux, *Mesoscopic Physics of Electrons and Photons* (Cambridge University Press, Cambridge, 2007).

[S2] B. Shapiro, Phys. Rev. Lett. **83**, 4733 (1999).

[S3] B. Shapiro, Phys. Rev. Lett. **57**, 2168 (1986).

[S4] I. Freund and D. Eliyahu, Phys. Rev. A **45**, 6133 (1992).

[S5] P. Sebbah, R. Pnini and A.Z. Genack, Phys. Rev. E **62**, 7348 (2000).

[S6] M.J. Stephen and G. Cwilich, Phys. Rev. Lett. **59**, 285 (1987).

[S7] R. Pnini and B. Shapiro, Phys. Rev. B **39**, 6986 (1989).

[S8] A. Retzker and B. Shapiro, Pramana–J. Phys. **58**, 225 (2002).

[S9] B.A. van Tiggelen and S.E. Skipetrov, Phys. Rev. E **73**, 045601 (2006).

[S10] S.E. Skipetrov and R. Maynard, Phys. Rev. B **62**, 886 (2000).

[S11] J.F. de Boer, M.P. van Albada and A. Lagendijk, Phys. Rev. B **45**, 658 (1992)